Diagnostic and Interventional Imaging 102 (2021) 455–462

Original article/*Cancer imaging*

MRI-based traditional radiomics and computer-vision nomogram for predicting lymphovascular space invasion in endometrial carcinoma

Ling Long[a], Jianqing Sun[b], Liling Jiang[a], Yixin Hu[a], Lan Li[a], Yong Tan[a], Meimei Cao[a], Xiaosong Lan[a], Jiuquan Zhang[a,*]

[a] *Department of Radiology, Chongqing University Cancer Hospital & Chongqing Cancer Institute & Chongqing Cancer Hospital, 400030 Chongqing, PR China*
[b] *Shukun (Beijing) Technology Co., Ltd., Jinhui Bd, Qiyang Rd, 100102 Beijing, China*

ARTICLE INFO

Keywords:
Uterus
Endometrial neoplasm
Magnetic resonance imaging
Nomogram
Computer vision

ABSTRACT

Purpose: To determine the capabilities of MRI-based traditional radiomics and computer-vision (CV) nomogram for predicting lymphovascular space invasion (LVSI) in patients with endometrial carcinoma (EC).

Materials and methods: A total of 184 women (mean age, 52.9 ± 9.0 [SD] years; range, 28–82 years) with EC were retrospectively included. Traditional radiomics features and CV features were extracted from pre-operative T2-weighted and dynamic contrast-enhanced MR images. Two models (Model 1, the radiomics model; Model 2, adding CV radiomics signature into the Model 1) were built. The performance of the models was evaluated by the area under the curve (AUC) of the receiver operator characteristic (ROC) in the training and test cohorts. A nomogram based on clinicopathological metrics and radiomics signatures was developed. The predictive performance of the nomogram was assessed by AUC of the ROC in the training and test cohorts.

Results: For predicting LVSI, the AUC values of Model 1 in the training and test cohorts were 0.79 (95% confidence interval [CI]: 0.702–0.889; accuracy: 65.9%; sensitivity: 88.8%; specificity: 57.8%) and 0.75 (95% CI: 0.585–0.914; accuracy: 69.5%; sensitivity: 85.7%; specificity: 62.5%), respectively. The AUC values of Model 2 in the training and test cohorts were 0.93 (95% CI: 0.875–0.991; accuracy: 94.9%; sensitivity: 91.6%; specificity: 96.0%) and 0.81 (95% CI: 0.666–0.962; accuracy: 71.7%; sensitivity: 92.8%; specificity: 62.5%), respectively. The discriminative ability of Model 2 was significantly improved compared to Model 1 (Net Reclassification Improvement [NRI] = 0.21; $P = 0.04$). Based on histologic grade, FIGO stage, Rad-score and CV-score, AUC values of the nomogram to predict LVSI in the training and test cohorts were 0.98 (95% CI: 0.955–1; accuracy: 91.6%; sensitivity: 91.6%; specificity: 96.0%) and 0.92 (95% CI: 0.823–1; accuracy: 91.3%; sensitivity: 78.5%; specificity: 96.8%), respectively.

Conclusions: MRI-based traditional radiomics and computer-vision nomogram are useful for preoperative risk stratification in patients with EC and may facilitate better clinical decision-making.

1. Introduction

Endometrial cancer (EC) is the sixth most common malignancy worldwide and the most common gynecological malignancy among females in developed countries with an estimated 320,000 new cases worldwide every year [1,2]. Women with early-stage EC are treated mainly by surgery consisting of total hysterectomy and bilateral salpingo-oophorectomy with or without lymphadenectomy, and the overall survival is approximately 90%; adjuvant radiotherapy is used for stage I–II patients with high-risk factors and stage III lymph node-negative patients [2,3].

Lymphovascular space invasion (LVSI) is defined by the presence of cancer in lymphatic and/or vascular spaces within the uterine myometrium [4]. LVSI is an important prognostic factor and is an independent risk factor for lymph node metastasis and poor outcomes in EC [5]. As a positive LVSI status is associated with a high rate of para-aortic lymph node metastases, preoperative

Abbreviations: AUC, Area under the curve; CI, Confidence interval; CV, computer vision; DCE, Dynamic contrast-enhanced; DICOM, Digital imaging and medical communications; EC, Endometrial carcinoma; IBSI, Image biomarker standardization initiative; LVSI, Lymphovascular space invasion; MRI, Magnetic resonance imaging; NRI, Net reclassification improvement; ROI, Regions of interest; ROC, Receiver operating characteristic; SD, Standard deviation; T2WI, T2-weighted image.

* Corresponding author.
E-mail address: zhangjq_radiol@foxmail.com (J. Zhang).

https://doi.org/10.1016/j.diii.2021.02.008
2211-5684/

clarification of LVSI status may aid in clinical treatment decision-making, such as the resection of para-aortic lymph nodes, which is needed in patients with LVSI-positive tumors. Therefore, it is extremely important to assess LVSI accurately before surgery. In routine clinical practice, magnetic resonance imaging (MRI) is widely accepted as the imaging modality of choice for preoperative assessment of EC, as it can accurately evaluate the extent of local disease and depict extrauterine tumor spread [6,7]. However, LVSI cannot be assessed by MRI or biopsy before surgery and can currently be assessed only after surgical resection of the uterine corpus [8].

Recently, the study of radiomics has become a hot subject of research. As a noninvasive, quantitative and low-cost approach, radiomics can be used to evaluate tumor heterogeneity objectively and comprehensively by extracting and analyzing high-throughput quantitative features from medical images (*i.e.*, computed tomography, positron emission tomography or MRI) through data characterization algorithms [9]. Radiomics can relate image features to phenotypic or gene-protein features by building descriptive and predictive models, which have the potential to provide valuable information for tumor detection, differential diagnosis, and therapeutic response assessment in oncology [10–15]. However, most of the traditional radiomic features are susceptible to noise and shallow and low-order image features, which are defined by mathematical formulas [16]. Therefore, traditional radiomic features may not be sufficient to reveal tumor heterogeneity and to predict LVSI in patients with EC. To overcome these limitations, several new strategies such as computer vision (CV) have been proposed. Computer vision features (CVFs), which include local and global features, have been used widely in traditional image processing [17]. Compared to traditional features, CVFs have the advantages of being insensitive to noise as well as rotation invariant. These advantages have the potential to avoid the effects of noise that affect handcrafted features on CVFs. In addition, CVFs have been used for disease diagnosis and prognosis prediction in medical imaging [18,19]. To date, no studies study have used the CV signature for the prediction of LVSI in EC.

The purpose of this study was to determine the capabilities of MRI-based traditional radiomics and CV nomogram for predicting LVSI in patients with EC.

2. Materials and methods

2.1. Patients

This retrospective study was reviewed and approved by our institutional review board, and written informed consent was waived. From January 2014 to July 2020, 269 consecutive women with suspected EC who had undergone pelvic MRI before treatment were eligible for this study. Patients were excluded for the following reasons:

- maximal tumor diameter of less than 1 cm or tumors were not visualized on MRI ($n = 60$);
- lack of dynamic contrast-enhanced (DCE) imaging ($n = 5$);
- motion artifacts affecting the focus of the lesion in MRI ($n = 5$);
- lack of complete surgical pathology reports ($n = 8$);
- preoperative neoadjuvant therapy or chemoradiotherapy ($n = 7$).

The final study population comprised 184 women. A flowchart of the patient demographics and exclusion criteria is shown in Fig. 1.

2.2. MRI protocol

All MRI examinations were performed with a 1.5-T MRI scanner (Ingenia®, Philips Healthcare) by using an eight-element pelvic phased-array surface coil. MRI imaging examination included axial T1-weighted images; sagittal, axial oblique (perpendicular to the long axis of the uterus) T2-weighted images without fat saturation; axial T2-weighted fat-saturated images; and axial oblique DCE images (three phases: 18, 55, and 120 seconds after injection). The gadolinium-based contrast agent (gadoterate meglumine, Hengrui) was intravenously injected at a dose of 0.2 mL/kg at a rate of 2 mL/s with a power injector, followed by a 20 mL saline flush at a rate of 2 mL/s (Table 1).

2.3. Image segmentation and feature extraction

Digital imaging and communications in medicine (DICOM) images, including axial oblique T2-weighted and axial oblique DCE (the second phase, 55 seconds after injection) images were downloaded from our picture archive and communication system for

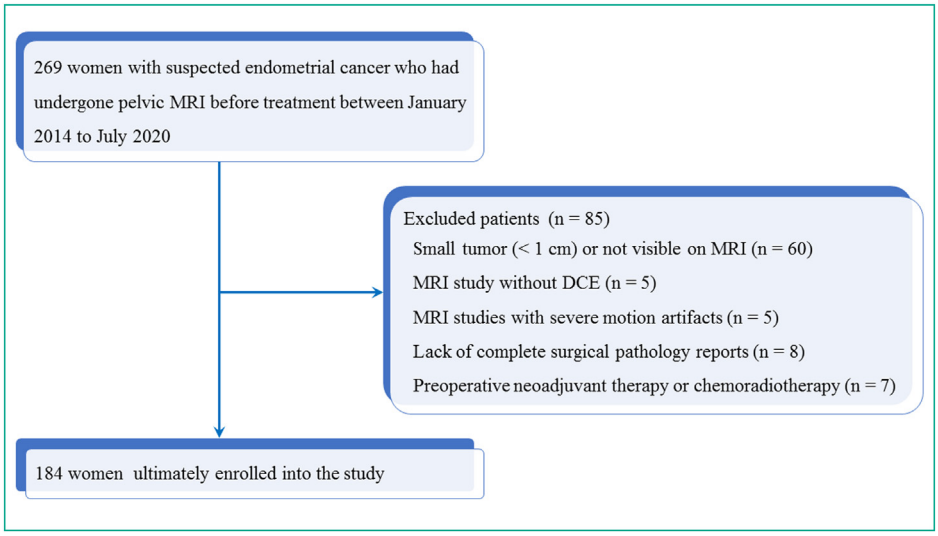

Fig. 1. Flow chart shows selection process of the study population and exclusion criteria.

Table 1
MRI protocol.

Parameters	Axial T1	Axial T2	Axial SPAIR T2	Sagittal T2	Axial oblique T2	Axial oblique DCE
TR (ms)	520	3000	3371	4722	2565	5.5
TE (ms)	10	100	80	100	100	1.71
Number of slices	24	24	24	24	24	140
Thickness (mm)	8	8	8	3	3	3.5
Acquisition matrix	40 × 330	280 × 409	280 × 317	252 × 252	552 × 501	252 × 180
FOV (mm)	250 × 380	250 × 380	250 × 380	250 × 250	220 × 380	250 × 380
Interslice gap	0.8	0.8	0.8	0	0	1.75
NSA	1	1	1	1	1	1
Flip angle (°)	90	90	90	90	90	15

DCE: Dynamic contrast-enhanced; TR: Repetition time; TE: Echo time; FOV: Field of view; NSA; No. of signals acquired. The axial oblique plane was perpendicular to the long axis of the uterus. Dynamic contrast-enhanced imaging was performed after intravenous administration of gadoterate meglumine (0.2 mL/kg) at a rate of 2 mL/s, followed by a 20 mL saline flush.

radiomic feature extraction. Two radiologists (L.L. and L.J., with 11- and 13 years of experience in pelvic MR imaging, respectively) used a Philips Radiomics Tool for manual segmentation but were blinded to the clinical and pathologic outcomes of the patients. The region of interest (ROI) covered the whole tumor and was delineated on both the T2-weighted and DCE images on each slice to generate two three-dimensional segmentations of the entire tumor. Diffusion-weighted imaging (DWI) was used as a reference for delineation.

According to the IBSI reference manual, image processing was standardized using in-house software. First, all images were normalized using the min-max scaling algorithm. Second, according to the IBSI reference manual, the feature category was defined. A complete set of radiomics features consisted of morphology (MORPH) features, local intensity (LI) features, intensity-based statistics (IS, STAT) features, intensity histogram (IH) features, intensity-volume histogram (IVH) features, gray level cooccurrence matrix (GLCM, CM) features, gray level run length matrix (GLRLM, RLM) features, gray level size zone matrix (GLSZM, SZM) features, gray level distance zone matrix (GLDZM, DZM) features, neighborhood gray tone difference matrix (NGTDM) features, and neighboring gray level dependence matrix (NGLDM) features [20,21]. Third, the high-level features were calculated using seven filters (including wavelet, logarithm, square, primitive, logarithm exponent, and square root). A total of 2420 radiomic features were extracted from each patient (Fig. 2). Four categories of CVFs were extracted from the segmented images, including:

- Local binary pattern (LBP);
- Histogram of oriented gradients (HOG);
- Speeded up robust features (SURF);
- Haar-like features.

In total, 9806 CVFs were computed based on Python 3.7 (https://www.python.org/) (Fig. 2).

To evaluate the reproducibility of the extracted feature values, 20 patients were randomly selected for tumor segmentation one month later by the same and one other radiologist. They both had no information or knowledge of the clinical and pathologic details. Subsequently, intraobserver consistency analysis was performed on the images drawn by the same radiologist, and interobserver consistency analysis was performed on the images drawn by both the radiologists.

2.4. Feature selection and model construction

The study population was randomly assigned to a training and test group at a ratio of 3:1 by stepwise sampling. Feature selection in the training group adopted a coarse-to-fine strategy. Mann-Whitney U test or paired Student *t* test was performed to compare the robust features between the LVSI-positive and LVSI-negative groups. All imaging features were ranked in ascending order in terms of the *P*-values of the features, and the top 5% were selected. Then, Pearson correlation coefficient (*r*) was computed between

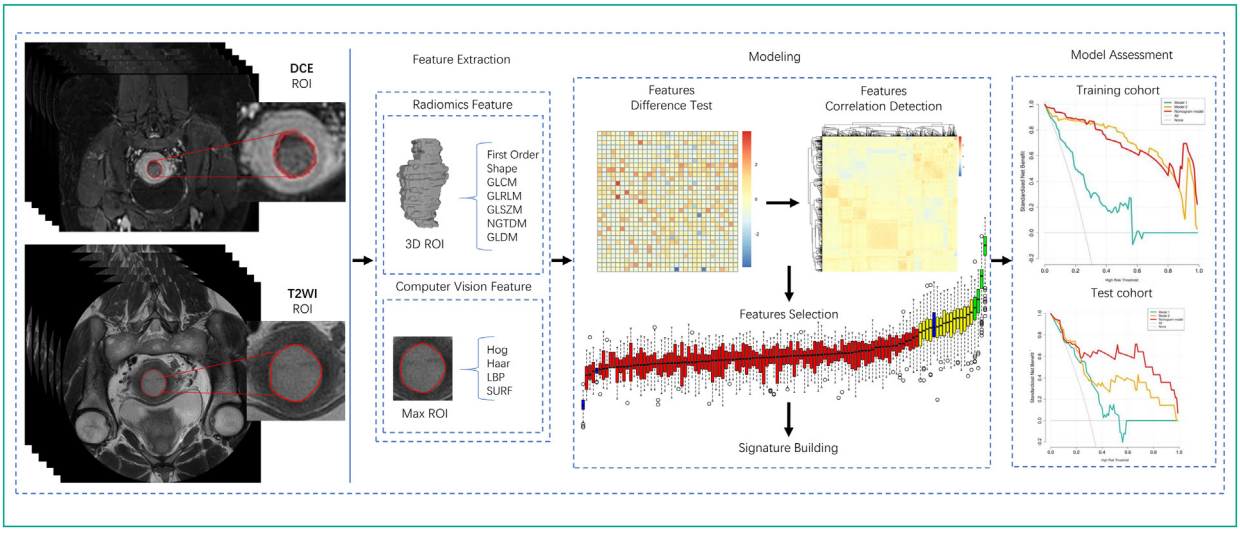

Fig. 2. Workflow of the model building process. Image segmentation was performed on dynamic contrast-enhanced (DCE) and T2-weighted (T2W) MR images. Traditional radiomics features were extracted from segmented images. For computer-vision features, images containing whole tumor were clipped from the segmented images. Computer-vision features were extracted from the largest level of the tumor.

each pair of features, with $|r| > 0.85$ and smaller *P*-values detected. Finally, the key features were detected for LVSI status prediction by using the Boruta algorithm, which is based on random forest. The feature selection strategy was applied to the handcrafted and CV radiomics feature selection process.

With the key features, a radial basis function kernel support vector machine (RBFSVM) was used to construct the models. A traditional radiomics model (called Model 1) was built using the handcrafted radiomics signature. Then, to evaluate the improved performance of the CV radiomics signature, the CV radiomics signature was added to Model 1 to form Model 2. The models were trained in the training group, and a 5-fold cross validation was used to determine the parameters of the models.

2.5. Model performance assessment

Net Reclassification Improvement (NRI) was used to measure the incremental prognostic value of model 2. Decision curve analysis (DCA) was used to evaluate the clinical usefulness of the models. The standardized net benefit (sNB) was derived from the decision curve.

2.6. Histological diagnosis analysis

All patients were surgicopathologically staged according to the 2009 FIGO staging system [22]. Hysterectomy specimens were sectioned along the longitudinal plane of the uterus, and myometrial invasion and cervical stromal invasion were estimated grossly and confirmed microscopically according to standard criteria. The uterus was sliced contiguously every 3–4 mm for pathologic analysis. Tumor histologic subtype, histologic grade (low, grade 1 or 2; high, grade 3 and nonendometrioid subtypes), presence of LVSI, myometrial invasion, cervical stromal invasion and metastasis in the sampled lymph nodes were confirmed microscopically.

2.7. Statistical analysis

All statistical analyses were performed with SPSS 22.0 software (IBM Corporation). Quantitative data were expressed as means ± standard deviation (SD) and ranges. Qualitative data were expressed as raw numbers, proportions and percentages. The two-way random effects model, single rater, absolute agreement intraclass correlation coefficient (ICC) was used to assess intraobserver and interobserver consistency, and an ICC > 0.75 was considered to indicate good agreement [23]. Differences in categorical variables were searched for using Chi-square ($\chi 2$) test and Mann-Whitney U test was used for continuous variables. Receiver operator characteristic (ROC) curves were used to evaluate the prediction identification performance in each model. A nomogram based on the Rad-score, CV-score and clinicopathological metrics was built into the training cohort to predict the potential for LVSI of EC and validated in the test cohort. The diagnostic performance of the nomogram was assessed using the ROC curve in the training cohort and the test cohort. All tests were two sided, and *P*-values < 0.05 were considered to be significant.

3. Results

3.1. Patient characteristics and surgical-histological results

A total of 184 women with a mean age of 52.9 ± 9.0 (SD) years (range: 28–82 years) were included. All patients underwent total hysterectomy, bilateral salpingo-oophorectomy and were surgicopathologically staged according to the 2009 FIGO staging system [22]. Of the 184 patients, 132/184 (71.7%) were FIGO stage I, 32/184 (17.4%) were FIGO stage II, 15/184 (8.2%) were FIGO stage III, and 5/184 (2.7%) were FIGO stage IV. In terms of grade, 117/184 EC (63.6%) were low grade and 67/184 (36.4%) were high grade. Patient clinicopathological findings are reported in Table 2. There were no significant differences between the two groups in terms of age ($P = 0.276$). The associations between LVSI and histologic grade and FIGO stage were significant ($P < 0.001$).

3.2. Interobserver agreement

The intraobserver ICCs ranged from 0.80 to 0.99. The interobserver ICCs ranged from 0.78 to 0.89, indicating good interobserver agreement.

3.3. Model development and performance

The key features of radiomics and CV are shown in Table 3. The performances of each predictive model are shown in Table 4. To predict LVSI, the AUC value of Model 1 in the training cohort was 0.79 (95% confidence interval [CI]: 0.702–0.889). The accuracy, sensitivity and specificity values of Model 1 and corresponding proportions and 95%CI in the training cohort were as follows: accuracy, 65.9% (91/138; 95%CI: 0.655–0.677); sensitivity, 88.8% (32/36) [0.874–0.905]; specificity, 57.8% (59/102; 95%CI: 0.576–0.603). The AUC value of Model 1 in the test cohort was 0.75 (95% CI: 0.585–0.914). The accuracy, sensitivity and specificity values of Model 1 and corresponding proportions and 95%CI in the test cohort were as follows: accuracy, 69.5% (32/46; 95%CI: 0.670–0.710); sensitivity: 85.7% (12/14; 95%CI: 0.827–0.890); specificity: 62.5% (20/32; 95%CI: 0.600–0.651). The AUC value of Model 2 in the training cohort was 0.93 (95% CI: 0.875–0.991). The accuracy, sensitivity and specificity values of Model 2 and corresponding proportions and 95%CI in the training cohort were as follows: accuracy, 94.9% (131/138; 95% CI: 0.945–0.955); sensitivity, 91.6% (33/36; 95% CI: 0.913–0.938); specificity: 96.0% (98/102; 95% CI: 0.954–0.964). The AUC value of Model 2 in the test cohort was 0.81 (95% CI: 0.666–0.962). The accuracy, sensitivity and specificity of model 2 and corresponding proportions and 95%CI in the test cohort were as follows: accuracy: 71.7% (33/46; 95% CI: 0.700–0.741); sensitivity: 92.8% (13/14; 95% CI: 0.926–0.964), specificity: 62.5% (20/32; 95% CI: 0.604–0.655). After adding the CV signature to Model 1 to form Model 2, the discriminative ability of Model 2 was significantly improved compared to Model 1 (NRI = 0.21, $P = 0.04$).

3.4. Clinical utility

To provide clinicians with an easy-to-use tool, the histologic grade, FIGO stage, Rad-score and CV-score were used to develop the nomogram in the training cohort (Fig. 3). The Hosmer-Lemeshow test indicated that there was no significant difference in each cohort (training cohort, $P = 0.15$; test cohort, $P = 0.81$), indicating that the nomogram was acceptable. The calibration curve of the nomogram for the possibility of LVSI positive is shown in Fig. 4. The DCAs indicated that model 2 and the nomogram were beneficial for predicting LVSI; model 2 obtains a higher sNB than model 1 within certain ranges of the risk threshold (Fig. 5). The AUC values of the nomogram for predict LVSI in the training and test cohorts were 0.98 (95% CI: 0.955–1; accuracy: 91.6%; sensitivity: 91.6%; specificity: 96.0%) and 0.92 (95% CI: 0.823–1; accuracy: 91.3%; sensitivity: 78.5%; specificity: 96.8%), respectively.

4. Discussion

In our study, we developed and validated predictive models for LVSI in patients with EC, including model 1 (traditional handcrafted radiomics signature), model 2 (CV radiomics signature was added

Table 2
Characteristics of 184 women with endometrial carcinoma.

Variable	LVSI (+) (n = 50)	LVSI (−) (n = 134)	P-value
Age (years)	53.3 ± 8.5 [33–82]	53.6 ± 9.1 [28–81]	0.276
Grade (%)			**< 0.001**
Low grade	19 (19/50; 38.0%)	98 (98/134; 73.1%)	
High grade	31 (31/50; 62.0%)	36 (36/134; 26.9%)	
FIGO stage (%)			**< 0.001**
I	24 (24/50; 48.0%)	108 (108/134; 80.6%)	
II	11 (11/50; 22.0%)	21 (21/134; 15.7%)	
III	11 (11/50; 22.0%)	4 (4/134; 3.0%)	
IV	4 (4/50; 8.0%)	1 (1/134; 0.7%)	

LVSI: lymphovascular space invasion; FIGO: International Federation of Gynecology and Obstetrics classification. Quantitative variables are expressed as means ± standard deviation; numbers in brackets are ranges. Qualitative data are expressed as raw numbers; numbers in parentheses are proportions followed by percentages. Bold indicates significant P values.

Table 3
Features for constructing model.

Traditional radiomic features	CV Features
Feature name	
DCE_WaveletFirstOrder_wavelet-LLH_TotalEnergy	DCE_haar2059
DCE_WaveletGLCM_wavelet-LLH_Correlation	DCE_haar3718
DCE_WaveletFirstOrder_wavelet-LLH_Minimum	DCE_haar2217
DCE_LogarithmGLDM_logarithm_SmallDependenceHighGrayLevelEmphasiss	DCE_haar2558
DCE_LogarithmGLDM_logarithm_LargeDependenceLowGrayLevelEmphasis	DCE_haar2933
DCE_LogarithmFirstOrder_logarithm_Range	T2WI_haar2288
DCE_SquareRootFirstOrder_squareroot_TotalEnergy	T2WI_haar3999
DCE_LogarithmGLSZM_logarithm_GrayLevelNonUniformityNormalized	T2WI_haar2324
DCE_LogarithmFirstOrder_logarithm_Median	T2WI_haar4005
T2WI_LogarithmGLRLM_logarithm_GrayLevelNonUniformityNormalized	T2WI_haar2151
T2WI_LogarithmNGTDM_logarithm_Coarseness	T2WI_haar3658

CV: computer-vision; DCE: Dynamic contrast-enhanced; T2WI: T2-weighted image.

Table 4
Performance of two predictive models in the training and test groups.

	AUC (95% CI)	Accuracy[a]	Sensitivity[a]	Specificity[a]
Model 1				
Training group	0.70 [0.702–0.889]	65.9 (91/138) [0.655–0.677]	88.8 (32/36) [0.874–0.905]	57.8 (59/102) [0.576–0.603]
Test group	0.75 [0.585–0.914]	69.5 (32/46) [0.670–0.710]	85.7 (12/14) [0.827–0.890]	62.5 (20/32) [0.600–0.651]
Model 2				
Training group	0.93 [0.875–0.991]	94.9 (131/138) [0.945–0.955]	91.6 (33/36) [0.913–0.938]	96.0 (98/102) [0.954–0.964]
Test group	0.81 [0.666–0.962]	71.7 (33/46) [0.700–0.741]	92.8 (13/14) [0.926–0.964]	62.5 (20/32) [0.604–0.655]

AUC: Area under the receiver operating characteristic curve; CI: Confidence interval.
[a] Accuracies, sensitivities and specificities are expressed in percentages; numbers in parentheses are proportions; numbers in brackets are 95% confidence intervals.

to model 1 to form model 2). Our findings suggest that the predictive value of model 2 for LVSI is higher than that of model 1, indicating that the addition of CV features can improve the prediction ability of LVSI in patients with EC.

LVSI is an independent prognostic for EC. Some previous studies reported that the 5-year survival rates of LVSI-positive and LVSI-negative patients were 64.5% and 83%, respectively, and deaths occurred in 26.7% of the patients with clinical stage I disease who had LVSI, compared with 9.1% in those without LVSI [24,25]. Predicting LVSI before surgery is important, as it can avoid overtreatment and lead to the selection of appropriate personalized treatment options, such as the resection of para-aortic lymph nodes [26]. As a noninvasive examination method, MRI is currently the main preoperative assessment method for EC. However, LVSI cannot be assessed by MRI or biopsy before surgery and can be assessed only after surgical resection of the uterine corpus.

In our study, we extracted traditional handcrafted radiomics features and CVFs of primary tumors and constructed a radiomics model to investigate the potential to predict LVSI in EC. T2W and DCE images can accurately delineate tumor boundaries. Hence, we extracted quantitative radiomic features of tumors using both T2W and DCE images.

Ueno et al. used an MRI-based radiomics model to identify LVSI in EC [27]. For identifying LVSI, the AUC and accuracy values were 0.80 and 76.6%, respectively. Although the effect of their handcrafted radiomics model was superior to model 1 of our research, their results lack an independent validation set for model validation. In contrast, a recent study by Bereby-Kahane et al. explored the capabilities of MRI-based texture analysis features to identify LVSI in EC, obtaining an AUC of 0.59 (sensitivity = 71%; specificity = 59%), suggesting that the predictive value of texture analysis for LVSI is limited [28]. The reason for this contradictory conclusion may be that this study included only 73 patients [28].

CVFs have been used widely in image processing. Some studies have suggested that CV features are valuable for predicting lymph node metastasis and disease diagnosis [17,18,29]. In our study, we extracted CVFs for the first time to build a model for predicting LVSI in EC. When the CV radiomics signature was added to the traditional radiomics signature, model 2 achieved encouraging performance in both the training cohort (AUC = 0.93) and the test cohort (AUC = 0.81). The value of model 2 in predicting LVSI was higher than that of model 1, and the discriminative ability of model 2 was significantly improved compared to that of model 1 (NRI = 0.21; P = 0.04). Our decision curve showed that model 2

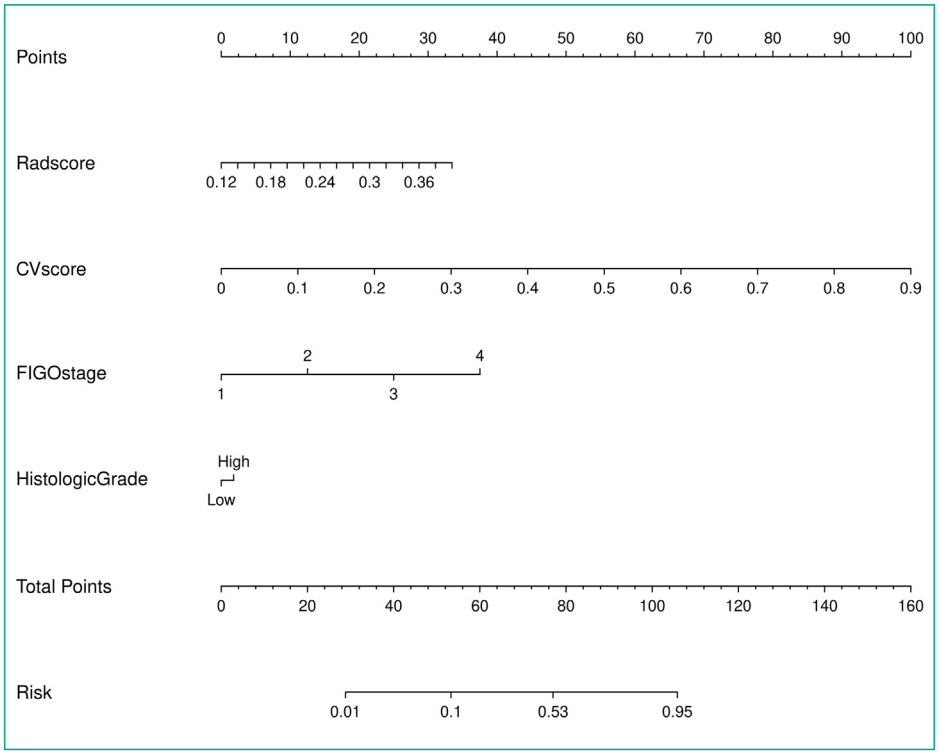

Fig. 3. Figure shows nomogram for predicting lymphovascular space invasion in patients with endometrial carcinoma.

can add more benefit to predicting LVSI than model 1, and it may be supported as a potentially useful tool to help treatment decision-making in clinical settings. The reason is that local features of CV excel in low computational complexity, since there is no prelearning process, no additional parameters to learn and they are highly robust to noise. A recent study carried out by Kailasam et al. also pointed out that local feature-based CV has the potential to provide relevant candidate diagnosis results for radiologists, which indicates that CV may make full use of texture, shape, and contour information to quantify the heterogeneity of tumors [29]. A previous study showed that CV features extracted from CT images combined with traditional radiomic features had potentially improved survival prediction ability in patients with esophageal squamous cell carcinoma [17]. In brief, the CV radiomics signature may be able to obtain more detailed information about tumors that cannot be mathematically defined.

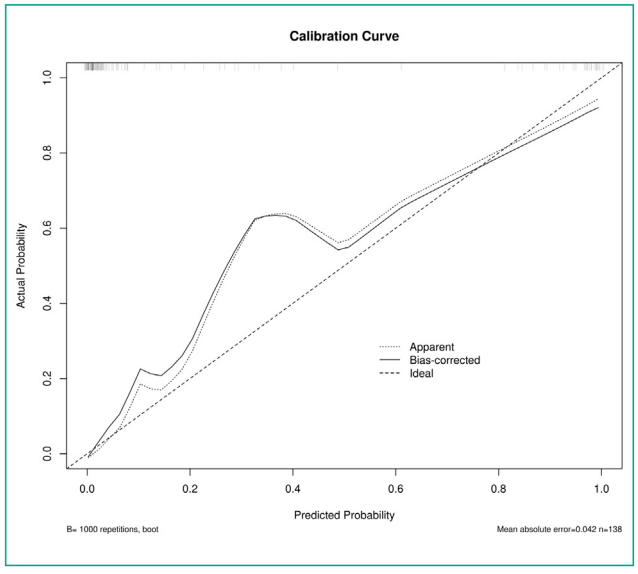

Fig. 4. Graph shows calibration curve of the nomogram.

Furthermore, we developed and validated a nomogram that incorporates the four items of Rad-score, CV-score, histologic grade, and FIGO stage, which showed excellent discrimination in the training and validation cohorts with AUCs of 0.98 and 0.92, respectively. The nomogram associated these independent variables and evaluated the risk of LVSI-positive status in each patient, which may facilitate better clinical decision-making. Luo Y et al. developed a nomogram algorithm consisting of the Rad-score, age, and tumor grade, which showed good predictive ability in predicting LVSI of EC preoperatively and presented AUCs of 0.820 and 0.807 in the training and test cohorts, respectively [30]. Compared with the previous study, a newly added CV score to our nomogram model, and the diagnostic efficacy of our nomogram model is higher than that of the previous study.

There are some limitations to our study. First, MR images did not include DWI, and DWI is more likely to produce artifacts because of the influence of the pelvis, so the inclusion of DWI analysis may be counterproductive. Second, all data in the present study were derived from the same institution, which needs to be further verified by multiple center validations. In the future, an attempt will be made to explore the performance of adding this factor in our research.

In conclusion, this study added the CV signature to develop a nomogram model for LVSI in patients with EC, which showed better predictive performance and clinical applicability.

Human rights

The authors declare that the work described has been carried out in accordance with the Declaration of Helsinki of the World Medical Association revised in 2013 for experiments involving humans.

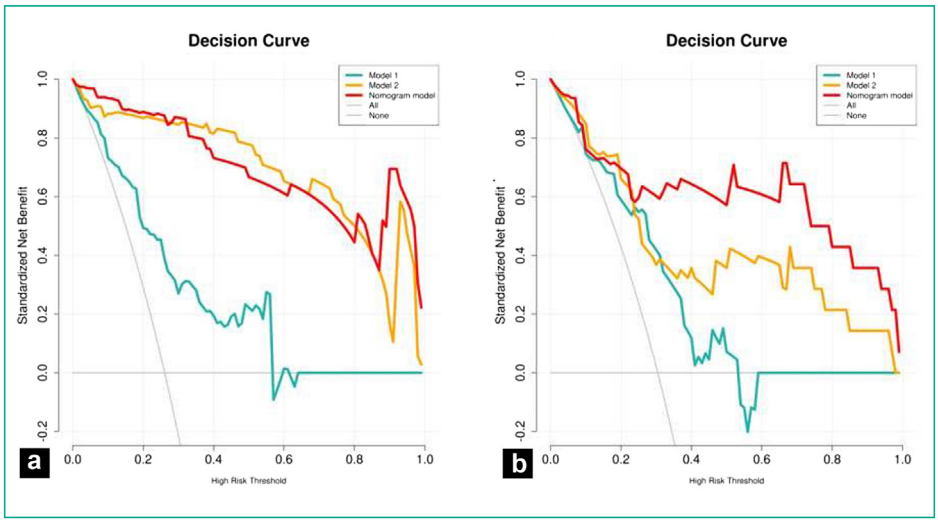

Fig. 5. Graph shows decision curves of each model for predicting lymphovascular space invasion in the training (a) and test cohorts (b).

Informed consent and patient details

This retrospective study was reviewed and approved by our institutional review board, and written informed consent was waived. The authors declare that this report does not contain any personal information that could lead to the identification of the patients.

Funding

This study has received funding by the National Natural Science Foundation of China (Grant No. 82071883), the combination projects of medicine and engineering of the Fundamental Research Funds for the Central Universities in 2019 (Project No. 2019CDY-GYB008), the Chongqing key medical research project of the combination of science and medicine (Grant No. 2019ZDXM007), and the 2019 SKY Imaging Research Fund of the Chinese International Medical Foundation (Project No. Z-2014-07-1912-10).

Author contributions

All authors attest that they meet the current International Committee of Medical Journal Editors (ICMJE) criteria for Authorship.

Credit Author Statement

Ling Long: Conceptualization, Writing- Original draft.
Jianqing Sun: Software, Methodology.
Liling Jiang: Formal analysis.
Yixin Hu: Investigation.
Lan Li: Project administration.
Yong Tan: Supervision,
Meimei Cao: Data Curation.
Xiaosong Lan: Methodology.
Jiuquan Zhang: Resources, Writing - Review & Editing, Funding acquisition.

Disclosure of interest

The authors declare that they have no competing interest.

References

[1] Torre LA, Bray F, Siegel RL, Ferlay J, Lortet-Tieulent J, Jemal A. Global cancer statistics, 2012. CA Cancer J Clin 2015;65:87–8.
[2] Amant F, Mirza MR, Koskas M, Creutzberg CL. Cancer of the corpus uteri. Int J Gynaecol Obstet 2018;143:37–50.
[3] Colombo N, Creutzberg C, Amant F, Bosse T, González-Martín A, Ledermann J, et al. ESMO-ESGO-ESTRO Consensus Conference on Endometrial Cancer: diagnosis, treatment and follow-up. Ann Oncol 2016;27:16–41.
[4] Bosse T, Peters EE, Creutzberg CL, Jürgenliemk-Schulz IM, Jobsen JJ, Mens JW, et al. Substantial lymph-vascular space invasion (LVSI) is a significant risk factor for recurrence in endometrial cancer: a pooled analysis of PORTEC 1 and 2 trials. Eur J Cancer 2015;51:1742–50.
[5] Guntupalli SR, Zighelboim I, Kizer NT, Zhang Q, Powell MA, Thaker PH, et al. Lymphovascular space invasion is an independent risk factor for nodal disease and poor outcomes in endometrioid endometrial cancer. Gynecol Oncol 2012;124:31–5.
[6] Sala E, Rockall A, Kubik-Huch RA. Advances in magnetic resonance imaging of endometrial cancer. Eur Radiol 2011;21:468–73.
[7] Nougaret S, Horta M, Sala E, Lakhman Y, Thomassin-Naggara I, Kido A, et al. Endometrial cancer MRI staging: updated guidelines of the European Society of Urogenital Radiology. Eur Radiol 2019;29:792–805.
[8] Braun MM, Overbeek-Wager EA, Grumbo RJ. Diagnosis and management of endometrial cancer. Am Fam Physician 2016;93:468–74.
[9] Lambin P, Rios-Velazquez E, Leijenaar R, Carvalho S, van Stiphout RG, Granton P, et al. Radiomics: extracting more information from medical images using advanced feature analysis. Eur J Cancer 2012;48:441–6.
[10] Kumar V, Gu Y, Basu S, Berglund A, Eschrich SA, Schabath MB, et al. Radiomics: the process and the challenges. Magn Reson Imaging 2012;30:1234–48.
[11] Aerts HJ, Velazquez ER, Leijenaar RT, Parmar C, Grossmann P, Carvalho S, et al. Decoding tumour phenotype by noninvasive imaging using a quantitative radiomics approach. Nat Commun 2014;5:4006.
[12] Wu W, Parmar C, Grossmann P, Quackenbush J, Lambin P, Bussink J, et al. Exploratory study to identify radiomics classifiers for lung cancer histology. Front Oncol 2016;6:71.
[13] Kickingereder P, Burth S, Wick A, Götz M, Eidel O, Schlemmer HP, et al. Radiomic profiling of glioblastoma: identifying an imaging predictor of patient survival with improved performance over established clinical and radiologic risk models. Radiology 2016;280:880–9.
[14] Antunes J, Viswanath S, Rusu M, Valls L, Hoimes C, Avril N, et al. Radiomics analysis on FLT-PET/MRI for characterization of early treatment response in renal cell carcinoma: a proof-of-concept study. Transl Oncol 2016;9:155–62.
[15] Lee S-H, Park H, Ko ES. Radiomics in breast imaging from techniques to clinical applications: a review. Korean J Radiol 2020;21:779–92.
[16] Suzuki K. Overview of deep learning in medical imaging. Radiol Phys Technol 2017;10:257–73.
[17] Wu L, Yang X, Cao W, Zhao K, Li W, Ye W, et al. Multiple level CT radiomics features preoperatively predict lymph node metastasis in esophageal cancer: a multicenter retrospective Study. Front Oncol 2019;9:1548.
[18] Friedman RJ, Gutkowicz-Krusin D, Farber MJ, Warycha M, Schneider-Kels L, Papastathis N, et al. The diagnostic performance of expert dermoscopists vs a computer-vision system on small-diameter melanomas. Arch Dermatol 2008;144:476–82.

[19] Ergin S, Kilinc O. A new feature extraction framework based on wavelets for breast cancer diagnosis. Comput Bio Med 2014;51:171–82.
[20] Zwanenburg A, Vallières M, Abdalah MA, Aerts H, Andrearczyk V, Apte A, et al. The image biomarker standardization initiative: standardized quantitative radiomics for high-throughput image-based phenotyping. Radiology 2020;295:328–38.
[21] Nakaura T, Higaki T, Awai K, Ikeda O, Yamashita Y. A primer for understanding radiology articles about machine learning and deep learning. Diagn Interv Imaging 2020;101:765–70.
[22] Creasman W. Revised FIGO staging for carcinoma of the endometrium. Int J Gynaecol Obstet 2009;105:109.
[23] Benchoufi M, Matzner-Lober E, Molinari N, Jannot AS, Soyer P. Interobserver agreement issues in radiology. Diagn Interv Imaging 2020;101:639–41.
[24] Abeler VM, Kjørstad KE, Berle E. Carcinoma of the endometrium in Norway: a histopathological and prognostic survey of a total population. Int J Gynecol Cancer 1992;2:9–22.
[25] Mariani A, Webb MJ, Galli L, Podratz KC. Potential therapeutic role of paraaortic lymphadenectomy in node-positive endometrial cancer. Gynecol Oncol 2000;76:348–56.
[26] Briët JM, Hollema H, Reesink N, Aalders JG, Mourits MJ, ten Hoor KA, et al. Lymphvascular space involvement: an independent prognostic factor in endometrial cancer. Gynecol Oncol 2005;96:799–804.
[27] Ueno Y, Forghani B, Forghani R, Dohan A, Zeng XZ, Chamming's F, et al. Endometrial carcinoma: MR imaging-based texture model for preoperative risk stratification: a preliminary analysis. Radiology 2017;284:748–57.
[28] Bereby-Kahane M, Dautry R, Matzner-Lober E, Cornelis F, Sebbag-Sfez D, Place V, et al. Prediction of tumor grade and lymphovascular space invasion in endometrial adenocarcinoma with MR imaging-based radiomic analysis. Diagn Interv Imaging 2020;101:401–11.
[29] Kailasam SP, Sathik MM. A novel hybrid feature extraction model for classification on pulmonary nodules. Asian Pac J Cancer Prev 2019;20:457–68.
[30] Luo Y, Mei D, Gong J, Zuo M, Guo X. Multiparametric MRI-based radiomics nomogram for predicting lymphovascular space invasion in endometrial carcinoma. J Magn Reson Imaging 2020;52:1257–62.